

Resurrection of the L - S coupling scheme in superdeformation

K. Sugawara-Tanabe,¹ A. Arima,² and N. Yoshida³

¹*Otsuma Women's University, Tama, Tokyo 206, Japan*

²*The Institute of Physical and Chemical Research, Wako, Saitama 351-01, Japan*

³*Faculty of Informatics, Kansai University, Takatsuki, Osaka 569, Japan*

(Received 16 August 1994)

In a realistic calculation the L - S coupling scheme is restored not only for the parity doublet levels but also for some other levels in the superdeformed limit, because of the strongly deformed quadrupole interaction. This real-spin mechanism can take into account the unique-parity level, in contrast to the pseudo-spin mechanism. The contribution from the unique-parity level to the $M1$ transition become non-negligible when the nucleus is superdeformed.

PACS number(s): 21.10.Ky, 21.10.Pc, 21.60.-n

I. INTRODUCTION

The motivation to start this work is the quantization of alignment [1] observed in the excited superdeformed bands ($\delta_{\text{osc}} \sim 0.6$) in the mass region of $A \sim 150$ and $A \sim 190$. On the other hand similar identical band structures are observed in the normally deformed nuclei [2], and recently also in the superdeformed band of $A \sim 130$ region [3] ($\delta_{\text{osc}} \sim 0.4$). When we look at the simple Nilsson diagram [4], we find the degeneracy of the parity-doublet levels (P - D) around $\delta_{\text{osc}} \sim 0.6$, i.e., the pair levels with asymptotic quantum numbers $[N, n_z = N, \Lambda = 0]_{\frac{1}{2}}$ and $[N - 1, n_z = N - 2, \Lambda = 1]_{\frac{1}{2}}$. The former level belongs to the unique-parity level with $\Omega = \frac{1}{2}$ (unique-parity partner), and the latter level to the pseudo-spin family as $[\tilde{N} - 2, \tilde{N} - 2, \tilde{0}]_{\frac{1}{2}}$ in the pseudo-spin representation [5, 6] with no pseudo-spin pair partner (pseudo-spin partner). Previously, we showed in a simple model [7] that the expectation values of the spin-orbit force by the P - D levels at $\delta_{\text{osc}} \sim 0.6$ converge to the values given by the asymptotic wave functions, which indicates the revival of the L - S coupling scheme.

In this paper we perform a more realistic calculation using the Nicra code [8], and find that the L - S coupling scheme is restored not only for the P - D levels, but also for the other levels in $N_{\text{sh}} = 2n_{\perp} + n_z$. Although the expectation values of the spin-orbit interaction for the unique-parity partners of the P - D levels do not converge well to the asymptotic values, their L - S coupled spherical-basis wave function components yield 85% of the total at superdeformation. Once the L - S coupling scheme works again, the quantization of alignment is explained by the real spin s . We call this mechanism real-spin mechanism in contrast to the pseudo-spin mechanism.

In Sec. II we calculate the expectation values of \mathbf{ls} and J_x for the eigenstates obtained from the exact diagonalization of H using the Nicra code [8]. In Sec. III we expand this eigenstate in terms of the spherical L - S coupled wave functions and compare the magnitude and the phases of the components. In Sec. IV we calculate the $M1$ transition rate between the eigenstates and estimate the contribution from the unique-parity level. In Sec. V we give our conclusions.

II. SPIN-ORBIT INTERACTION AND ALIGNMENT

We use the Nilsson Hamiltonian [9] which is assumed to have an axially symmetry with a rational ratio $a:b$ between the frequencies ω_{\perp} and ω_z .

$$H = -\frac{\hbar^2}{2M} \nabla^2 + \frac{M}{2} [\omega_{\perp}^2 (x^2 + y^2) + \omega_z^2 z^2] + \xi_{ll} (l^2 - \langle l^2 \rangle_N) + \xi_{ls} \mathbf{ls}, \quad (1)$$

where the volume conservation condition is used;

$$\omega_{\perp} = a\omega_{\text{sh}}, \quad \omega_z = b\omega_{\text{sh}}, \quad \omega_{\text{sh}} = \omega_0 (a^2 b)^{-1/3} \quad (2)$$

$$\hbar\omega_0 = 41A^{-1/3} \text{ MeV}.$$

The deformation parameter δ_{osc} is given by $3(a-b)/(2a+b)$. An energy eigenvalue of H without the residual l^2 and \mathbf{ls} interactions is described by $\hbar\omega_{\text{sh}}(N_{\text{sh}} + a + \frac{b}{2})$ with the shell quantum number $N_{\text{sh}} = an_{\perp} + bn_z$, $n_{\perp} = n_{+} + n_{-}$, $\Lambda = n_{+} - n_{-}$ and n_i is the eigenvalue of $c_i^{\dagger}c_i$ ($i = +, -$ or z of the harmonic-oscillator bosons [7]). The corresponding eigenfunction is a so-called asymptotic wave function which is usually denoted by the quantum numbers $[Nn_z\Lambda]\Omega$. In the superdeformed shape where $a:b = 2:1$, the P - D levels belong to the same $N_{\text{sh}} = 2n_{\perp} + n_z$ with the same shell energy $\hbar\omega_{\text{sh}}(N_{\text{sh}} + 5/2)$, which indicates that the P - D levels are almost degenerate in energy. This energy degeneracy is not destroyed in the realistic calculation, because the residual interactions (l^2 and \mathbf{ls}) are much smaller than the harmonic-oscillator potential. From now on we take $N_{\text{sh}} = 6(7)$ for the proton shell (neutron shell) of ^{152}Dy and $N_{\text{sh}} = 7(8)$ for the proton shell (neutron shell) of ^{192}Hg , because the fermi surface is located near these shells at superdeformation for these nuclei. For the $A \sim 130$ region, $a:b = 3:2$ and $N_{\text{sh}} = 3n_{\perp} + 2n_z$. Again the energy degeneracy is found for $[550]_{\frac{1}{2}}$ and $[420]_{\frac{1}{2}}$ in the proton shell and $[660]_{\frac{1}{2}}$ and $[530]_{\frac{1}{2}}$ in the neutron shell around $\delta_{\text{osc}} = 0.3 \sim 0.4$ near the fermi surface of 58 and 74 in the Nilsson diagram. Since the shell energy is much smaller in this case, the

shell gap is not clear, but we can still see the degeneracy of some levels.

The eigenvector of (1) is given by

$$H|\sigma, \Omega, \alpha\rangle = E(\sigma, \Omega, \alpha)|\sigma, \Omega, \alpha\rangle, \quad (3)$$

where $\Omega = \Lambda + \Sigma (= \frac{1}{2}$ for the P - D levels), α denotes the signature, and σ represents all the other quantum numbers. In Figs. 1 and 2 we show the energy eigenvalues of the P - D levels together with the other levels belonging to the same N_{sh} around $\delta_{osc} \sim 0.6$. These results were obtained using the NICRA code [8] with the parameters given in Table I. We plot the positive and negative parity levels in different figures next to each other with the same scale of ordinate for both of proton and neutron shells. The solid lines correspond to the P - D levels. In-

side of the figures $E(\sigma, \Omega, \alpha)$ is labeled by the asymptotic quantum numbers $Nn_z\Lambda\Omega$. Although the P - D levels are plotted in different figures in order to get rid of mess, one sees the P - D levels cross each other and the levels belonging to the same N_{sh} come near to this crossing around superdeformation, because of the same scale of ordinate. As there is no cranking term in (1), energy eigenvalues are degenerate with respect to signatures.

We calculated the expectation values of the angular momentum J_x using the eigenfunctions from (3), i.e., $\langle\sigma, \Omega, \alpha|J_x|\sigma, \Omega, \alpha\rangle$, and of the spin-orbit force, $\langle\sigma, \Omega, \alpha|ls|\sigma, \Omega, \alpha\rangle$. Figures 3 and 4 show these values for all the levels with $\Omega = \frac{1}{2}$ belonging to the same N_{sh} both for the proton shell (π) and the neutron shell (ν) of $A = 152$ and 192 cases, respectively. Inside of the figures the single-particle levels are identified by the asymptotic quantum numbers $Nn_z\Lambda$, where we drop Ω , as all levels have $\Omega = \frac{1}{2}$. In the figure we choose the signature which gives the positive values of $\langle\sigma, \Omega, \alpha|J_x|\sigma, \Omega, \alpha\rangle$ at $\delta_{osc} = 0.0$. The other signature

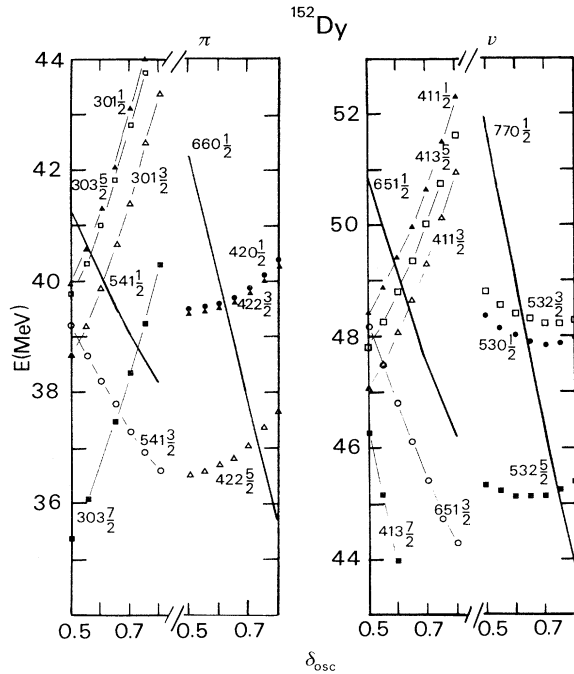


FIG. 1. The calculated energies $E(\sigma, \Omega, \alpha)$ near superdeformation for the P - D levels and the other levels belonging to the N_{sh} , as a function of the ellipsoidal deformation δ_{osc} for the proton shell (π) and the neutron shell (ν) in ^{152}Dy . The values of δ_{osc} run from 0.5 to 0.8. The ordinate is in units of MeV. All $E(\sigma, \Omega, \alpha)$ are obtained by diagonalizing the total H but are labeled by asymptotic quantum numbers $Nn_z\Lambda\Omega$, to which they converge at very large deformation. The P - D levels are denoted by the solid lines, i.e., $541\frac{1}{2}$ and $660\frac{1}{2}$ in the π shell and $651\frac{1}{2}$ and $770\frac{1}{2}$ in the ν shell. For the negative parity levels of the π shell, the open circles denote $541\frac{3}{2}$, the closed triangles $301\frac{1}{2}$, the open triangles $301\frac{3}{2}$, the closed squares $303\frac{7}{2}$ and the open squares $303\frac{5}{2}$. For the positive parity levels of the π shell, the closed circles denote $420\frac{1}{2}$, the closed triangles $422\frac{3}{2}$ and the open triangles $422\frac{5}{2}$. For the positive parity levels of the ν shell, the open circles denote $651\frac{3}{2}$, the closed triangles $411\frac{1}{2}$, the open triangles $411\frac{3}{2}$, the closed squares $413\frac{7}{2}$ and the open squares $413\frac{5}{2}$. For the negative parity levels of the ν shell, the closed circles denote $530\frac{1}{2}$, the closed squares $532\frac{5}{2}$ and the open squares $532\frac{3}{2}$.

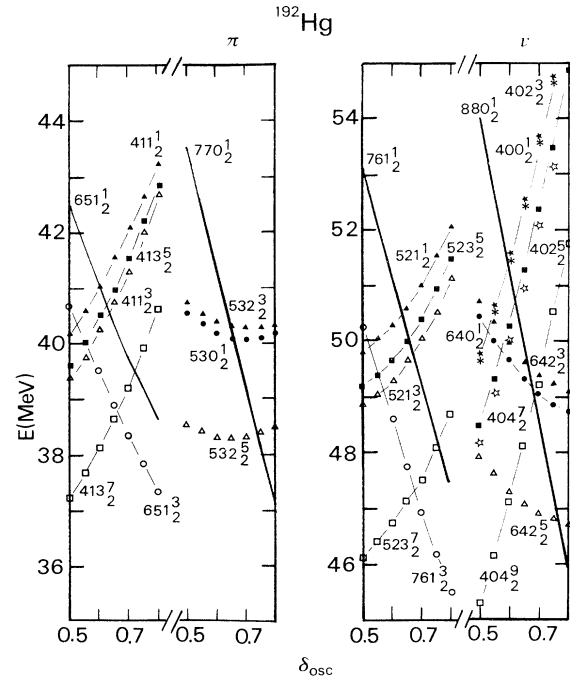


FIG. 2. The same quantities as in Fig. 1 for ^{192}Hg . The solid lines are the P - D levels, $651\frac{1}{2}$ and $770\frac{1}{2}$ for the proton (π) shell and $761\frac{1}{2}$ and $880\frac{1}{2}$ for the neutron (ν) shell. In the positive parity levels of the π shell, the open circles denote $651\frac{3}{2}$, the closed triangles $411\frac{1}{2}$, the open triangles $411\frac{3}{2}$, the closed squares $413\frac{5}{2}$ and the open squares $413\frac{7}{2}$. In the negative parity levels of the π shell, the closed circles denote $530\frac{1}{2}$, the closed triangles $532\frac{3}{2}$ and the open triangles $532\frac{5}{2}$. In the negative parity levels of the ν shell, the open circles denote $761\frac{3}{2}$, the closed triangles $521\frac{1}{2}$, the open triangles $521\frac{3}{2}$, the closed squares $523\frac{5}{2}$ and the open squares $523\frac{7}{2}$. In the positive parity levels of the ν shell, the closed circles denote $640\frac{1}{2}$, the closed triangles $642\frac{3}{2}$, the open triangles $642\frac{5}{2}$, the closed squares $404\frac{7}{2}$, the open squares $404\frac{5}{2}$, the closed stars $402\frac{3}{2}$, the open stars $402\frac{5}{2}$ and the asterisks $400\frac{1}{2}$.

TABLE I. The parameters for the Nilsson potential. The relations between ξ_{lu} and ξ_{ls} in Eq. (1), and κ and μ below are $\xi_{ls} = -2\kappa\hbar\omega_0$ and $\xi_{lu} = \mu\xi_{ls}/2$.

| N | Dy | | | | Hg | | | |
|-----|------------|---------|------------|---------|------------|---------|------------|---------|
| | κ_p | μ_p | κ_n | μ_n | κ_p | μ_p | κ_n | μ_n |
| 3 | 0.09 | 0.30 | 0.09 | 0.25 | 0.05 | 0.35 | 0.05 | 0.35 |
| 4 | 0.065 | 0.57 | 0.07 | 0.39 | 0.05 | 0.45 | 0.05 | 0.45 |
| 5 | 0.062 | 0.34 | 0.062 | 0.43 | 0.05 | 0.45 | 0.05 | 0.45 |
| 6 | 0.062 | 0.26 | 0.062 | 0.34 | 0.05 | 0.45 | 0.05 | 0.45 |
| 7 | 0.054 | 0.69 | 0.062 | 0.26 | 0.0635 | 0.3 | 0.0635 | 0.3 |
| 8 | 0.054 | 0.69 | 0.062 | 0.26 | 0.0635 | 0.3 | 0.0635 | 0.3 |

partner gives the same amount with a negative sign. The values of $\langle\sigma, \Omega, \alpha | \mathbf{ls} | \sigma, \Omega, \alpha\rangle$ are degenerate with respect to signature. We see these expectation values tend to decrease with increasing deformation for both Dy and Hg. It is very remarkable that all of the single-particle expectation values, except for the unique-parity partner of the P - D levels, approach the values given by the asymptotic wave functions, i.e., $\langle\sigma, \Omega, \alpha | \mathbf{ls} | \sigma, \Omega, \alpha\rangle$ approaches $\Lambda\Sigma$ and $\langle\sigma, \Omega = \frac{1}{2}, \alpha | J_x | \sigma, \Omega = \frac{1}{2}, \alpha\rangle$ approaches $\pm\frac{1}{2}$. This

indicates that the L - S coupling scheme¹ is already recovered for these levels. As for the unique-parity partners of the P - D levels, they do show a tendency to reach the asymptotic values, but not yet enough even at $\delta_{\text{osc}} \sim 0.8$. We will return to this point later.

This feature that the expectation values of the \mathbf{ls} interaction converge to the asymptotic values in the superdeformed limit is characteristic not only of the levels with $\Omega = \frac{1}{2}$, but also of some other single-particle levels with larger Ω in the same limit [7]. In Fig. 5 we calculate

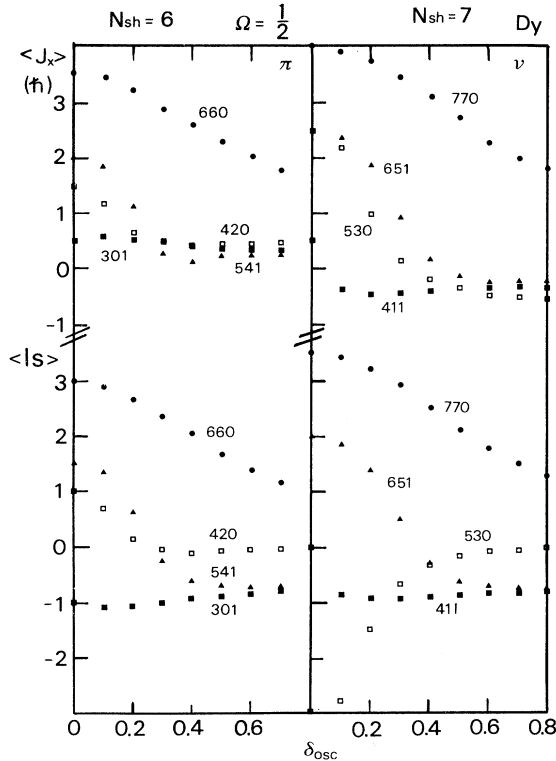


FIG. 3. The expectation values of J_x and \mathbf{ls} by the eigenstate $|\sigma, \Omega = \frac{1}{2}, \alpha\rangle$ belonging to the same $N_{\text{sh}} = 6$ for the proton shell (π) and 7 for the neutron shell (ν) in ^{152}Dy . The ordinate is in units of \hbar . The state $|\sigma, \Omega, \alpha\rangle$ is obtained by diagonalizing the total H , but labeled by the asymptotic quantum numbers N, n_z, Λ . For the expectation values of J_x , we choose the signature that gives the positive values of $\langle\sigma, \Omega = \frac{1}{2}, \alpha | J_x | \sigma, \Omega = \frac{1}{2}, \alpha\rangle$ at $\delta_{\text{osc}} = 0$. For the π shell δ_{osc} is from 0 to 0.7 and the ν shell δ_{osc} is from 0 to 0.8.

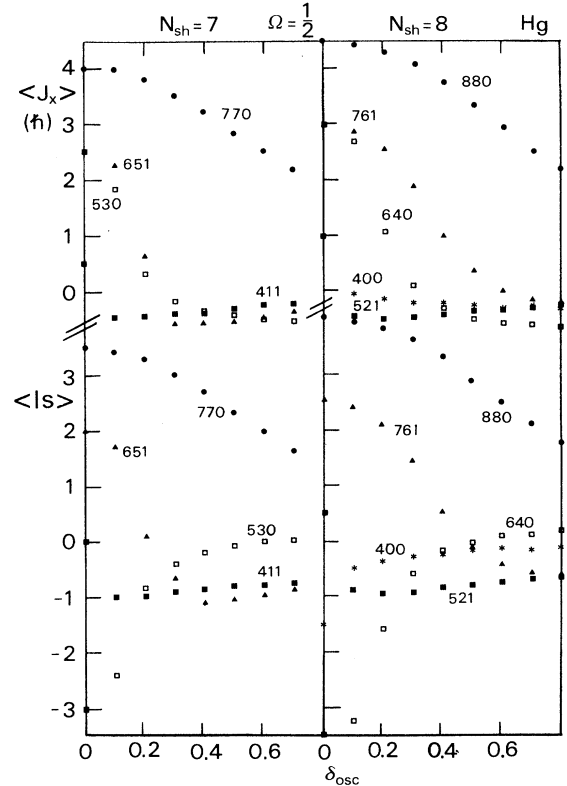


FIG. 4. The same quantities as in Fig. 3 for ^{192}Hg . $N_{\text{sh}} = 7$ for the proton shell (π) and 8 for the neutron shell (ν).

¹Here the L - S coupling scheme means Λ and Σ become good quantum numbers.

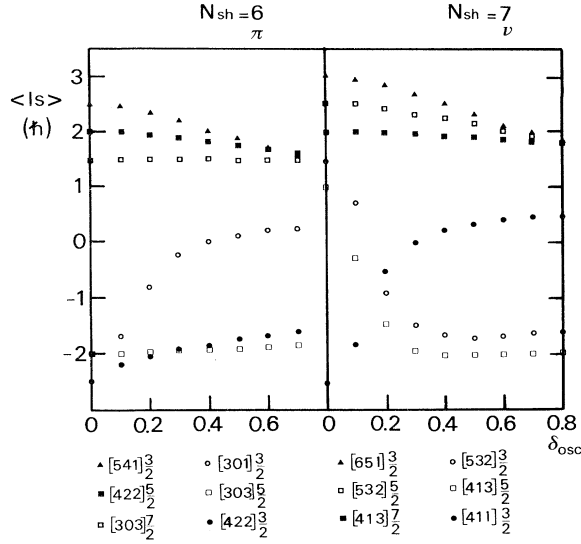


FIG. 5. The expectation values of \mathbf{ls} by all the levels except for $\Omega = \frac{1}{2}$ belonging to the same $N_{sh} = 6$ for the proton shell (π) and 7 for the neutron shell (ν) in ^{152}Dy . The ordinate is in units of \hbar . The symbols correspond to those labeled by the asymptotic quantum numbers $[Nn_z\Lambda]\Omega$, which are denoted under each figure of π and ν shells. In π shell, closed triangles denote $[541]_{\frac{3}{2}}^{\frac{3}{2}}$, closed squares $[422]_{\frac{5}{2}}^{\frac{5}{2}}$, open squares $[303]_{\frac{7}{2}}^{\frac{7}{2}}$, open circles $[301]_{\frac{3}{2}}^{\frac{3}{2}}$, open squares $[303]_{\frac{5}{2}}^{\frac{5}{2}}$ and closed circles $[422]_{\frac{3}{2}}^{\frac{3}{2}}$. In ν shell, closed triangles denote $[651]_{\frac{3}{2}}^{\frac{3}{2}}$, closed squares $[413]_{\frac{7}{2}}^{\frac{7}{2}}$, open squares $[532]_{\frac{5}{2}}^{\frac{5}{2}}$, open circles $[532]_{\frac{3}{2}}^{\frac{3}{2}}$, open squares $[413]_{\frac{5}{2}}^{\frac{5}{2}}$ and closed circles $[411]_{\frac{3}{2}}^{\frac{3}{2}}$. The abscissa is δ_{osc} , and δ_{osc} starts from 0 to 0.7 for the π shell, and from 0 to 0.8 for the ν shell.

$\langle \sigma, \Omega, \alpha | \mathbf{ls} | \sigma, \Omega, \alpha \rangle$ for the $N_{sh} = 6$ of the proton shell (π) and $N_{sh} = 7$ of the neutron shell (ν) for the ^{152}Dy . All levels show a tendency to converge to their asymptotic values, except $[541]_{\frac{3}{2}}^{\frac{3}{2}}$ in π , and $[651]_{\frac{3}{2}}^{\frac{3}{2}}$ and $[532]_{\frac{5}{2}}^{\frac{5}{2}}$ in ν which show a slow and incomplete convergence. These levels belong to the unique-parity levels with small Ω .

In Figs. 6 and 7 we show the effect of rotation on these expectation values by the P - D levels of Dy and Hg, respectively. In this case $|\sigma, \Omega, \alpha\rangle$ is the eigenstate of $H' = H - \hbar\omega_{rot}J_x$. So long as the rotational frequency $\hbar\omega_{rot}$ is small (≤ 0.3), the effect of the cranking is negligible, especially in the expectation values of \mathbf{ls} . This tendency agrees with the prediction given by the perturbation calculation [7]. As for the expectation values of J_x , those produced by one signature partner of the unique-parity level show a gradual increase with an increasing $\hbar\omega_{rot}$, while those coming from the other signature partner increase rapidly and approach the asymptotic values for $\delta_{osc} \sim 0.6$.

We also calculate the expectation values of \mathbf{ls} and J_x for the case of ^{132}Ce . These expectation values converge much faster than the Dy and Hg cases to the asymptotic values for $\delta_{osc} = 0.3 \sim 0.4$, except for the unique-parity levels with small Ω . However the quantization of alignment observed in ^{132}Ce is in the region of $\hbar\omega_{rot} \geq 0.5$ [3]. Under such a large cranking term, it is very hard to

see the detailed character of the wave function, which is discussed in the following section.

III. L - S COUPLED SPHERICAL WAVE FUNCTION

We now investigate the detailed character of the single-particle levels at superdeformation using spherical wave functions. The state $|\sigma, \Omega, \alpha\rangle$ is expanded by the L - S coupled spherical basis $|N, L, L_z = \Lambda, \Omega\rangle$ utilizing the formula

$$|\sigma, \Omega, \alpha\rangle = \sum W_{NLA\Omega}^{\sigma\Omega} |N, L, \Lambda, \Omega\rangle. \quad (4)$$

To make our study clear we show the coefficients of the P - D levels, i.e., $W_{NLA\Omega}^{\sigma\frac{1}{2}}$, as functions of δ_{osc} for ^{152}Dy in Figs. 8 (π) and 9 (ν). At the spherical limit the $\Lambda = 0$ and 1 components are mixed almost equally (0.54 to 0.46). This indicates j - j coupling is more suitable. With increasing δ_{osc} the dominant spherical components decrease, while the other components increase. Finally the amplitudes of the $\Lambda = 1$ ($\Lambda = 0$) components become dominant for the pseudo-spin partner (the unique-parity partner) of the P - D levels.

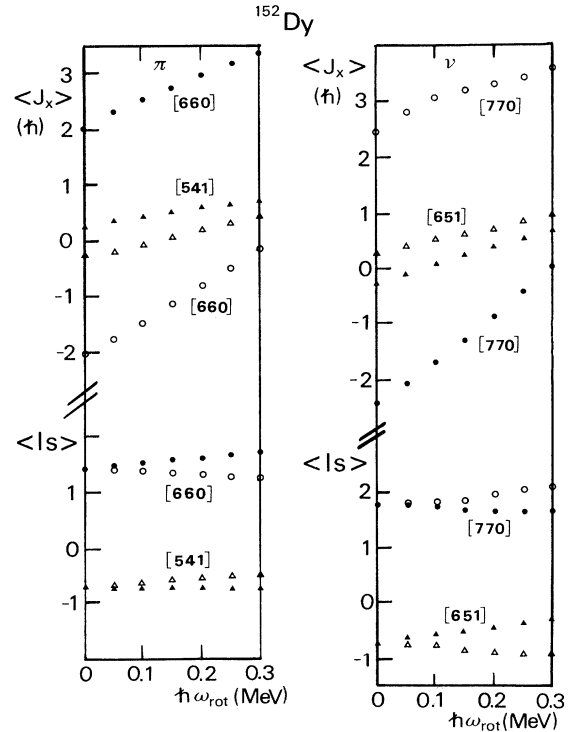
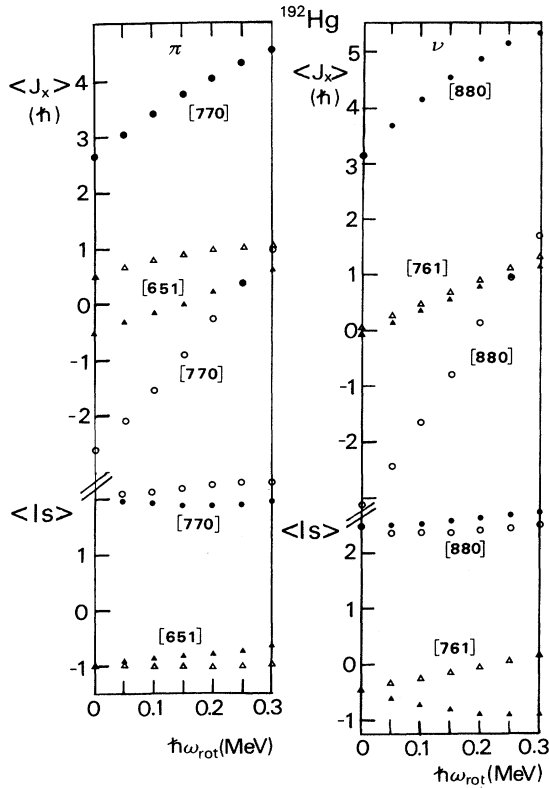


FIG. 6. The effect of the Coriolis interaction on $\langle \sigma, \Omega = \frac{1}{2}, \alpha | J_x | \sigma, \Omega = \frac{1}{2}, \alpha \rangle$ and $\langle \sigma, \Omega = \frac{1}{2}, \alpha | \mathbf{ls} | \sigma, \Omega = \frac{1}{2}, \alpha \rangle$ as functions of $\hbar\omega_{rot}$ for the P - D levels in ^{152}Dy at $\delta_{osc} = 0.6$. Here $|\sigma, \Omega, \alpha\rangle$ is the eigenfunction of $H' = H - \hbar\omega_{rot}J_x$. The symbols are labeled by the asymptotic quantum numbers $[Nn_z\Lambda]$. Open and closed symbols correspond to the different signatures with the same $[Nn_z\Lambda]\Omega$. The abscissa is $\hbar\omega_{rot}$, and it is from 0 to 0.3 in units of MeV.

FIG. 7. The same quantities as in Fig. 6 for ^{192}Hg .

We calculate the values of $\sum_L |W_{NL\Lambda\Omega}^{\sigma\Omega}|^2$ for both $\Lambda = 0$ and 1 and show them in Table II. For example, in the $[541]_{\frac{1}{2}}$ level of Fig. 8, the squares of the $\Lambda = 1$ components to those of $\Lambda = 0$ are 0.78 to 0.22 at $\delta_{osc}=0.6$, while at $\delta_{osc} = 0.2$ they are 0.23 to 0.77. For the state $[660]_{\frac{1}{2}}$, the squares of $\Lambda = 1$ components to those of $\Lambda = 0$ are 0.15 to 0.85 at $\delta_{osc} = 0.6$, while at $\delta_{osc} = 0.2$ they are 0.42 to 0.58. At $\delta_{osc} = 0.8$, $\sum_L |W_{NL\Lambda\Omega}^{\sigma\Omega}|^2$ of $\Lambda = 0$ becomes 91 ~ 92% for the unique-parity partner state of the P - D levels, while for $\Lambda = 1$ it is 84–89% for the pseudo-spin partner state. These results indicate that the L - S coupling scheme is restored in the superdeformed limit, and this resurrection is better for the unique-parity partner levels than for the pseudo-spin partner levels of the P - D levels, i.e., the unique-parity partner (the pseudo-spin partner) has 0.85(0.78) at $\delta_{osc} = 0.6$ for the proton shell and 0.81(0.69) for the neutron shell. Although the convergence of the expectation values of $|s|$ to the asymptotic limit, shown in Figs. 3–5, was worse for the unique-parity partner levels of the P - D levels, Table II illustrates that the L - S coupling scheme becomes better for the unique-parity partner of the P - D levels at $\delta_{osc}=0.6$. As seen in Figs. 8 and 9, the reason for this is that the amplitudes of $\Lambda = 0$ and those of $\Lambda = 1$ are out of phase for the $[541]_{\frac{1}{2}}$ and $[651]_{\frac{1}{2}}$, while they are in phase for the $[660]_{\frac{1}{2}}$ and $[770]_{\frac{1}{2}}$. The out-of-phase amplitudes between $\Lambda = 1$ and 0 cause the cancellation of the matrix element of $|s|$, and help the convergence to the asymptotic values. On the

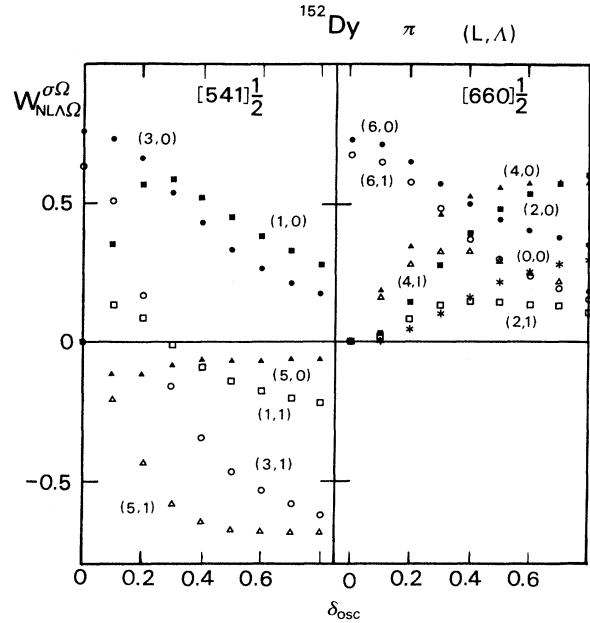


FIG. 8. The expansion coefficients of the P - D levels in the proton shell of ^{152}Dy in terms of the L - S coupled spherical basis $|NL\Lambda\Omega = \frac{1}{2}\rangle$ as functions of deformation. The filled (open) symbols denote the coefficients of $\Lambda = 0$ (1). All the symbols are labeled by the quantum numbers (L, Λ) . The quantum number $\Omega = \frac{1}{2}$ is common for all spherical basis in each figure. For $[541]_{\frac{1}{2}}$, the circles correspond to $L = 3$, the squares to $L = 1$ and the triangles to $L = 5$. For $[660]_{\frac{1}{2}}$, the circles correspond to $L = 6$, the squares to $L = 2$, the triangles to $L = 4$ and the asterisks denote the contribution from $s1/2$ ($L = 0, \Lambda = 0$). The abscissa is δ_{osc} from 0 to 0.8.

other hand the in-phase amplitude has no cancellation, and the convergence is slower. This is not only the case for the unique-parity partner level of the P - D levels, but also for the unique-parity levels with small Ω , which show in Fig. 5 a slow convergence to the asymptotic values. For example, $[541]_{\frac{1}{2}}$ in the proton shell has the ratio of the summed values of $\sum_L |W_{NL\Lambda\Omega}^{\sigma\Omega}|^2$ for $\Lambda = 1$ as 0.64:0.36 at $\delta_{osc} = 0.0$ and 0.89:0.11 at $\delta_{osc} = 0.6$. The neutron state $[532]_{\frac{5}{2}}$ ($[651]_{\frac{3}{2}}$) has the ratio of the summed values for $\Lambda = 2(1)$ to $3(2)$ as 0.90:0.10 (0.86:0.14) at $\delta_{osc} = 0.6$. The L - S coupling scheme is also restored for these levels in the superdeformed limit.

The reason why the L - S coupling scheme works well can be simply explained from the nature of the matrix elements of the axially symmetric deformed field δY_{20} . If we expand the state $|\sigma, \Omega, \alpha\rangle$ in terms of the spherical j - j coupled wave function $|N, l, j, \Omega\rangle$, instead of (4), there appear three kinds of matrix elements of Y_{20} . The matrix element of $(j' = l - 2 \pm \frac{1}{2}|Y_{20}|j = l \pm \frac{1}{2})$ is proportional to $l\sqrt{(l-1)(l+1)/[(2l-1)(2l+1)]}$. This is of comparable order to the diagonal element $(j' = l \pm \frac{1}{2}|Y_{20}|j = l \pm \frac{1}{2})$, which is proportional to $[\frac{3}{4} - j(j+1)]^2/[j(j+1)(2j+3)(2j-1)]$. On the other hand the matrix element between spin-orbit partners $(j' = 1 - \frac{1}{2}|Y_{20}|j = l + \frac{1}{2})$ is proportional to $\sqrt{(2j+1)(2j'+1)/[jj'(j+1)]}$, and

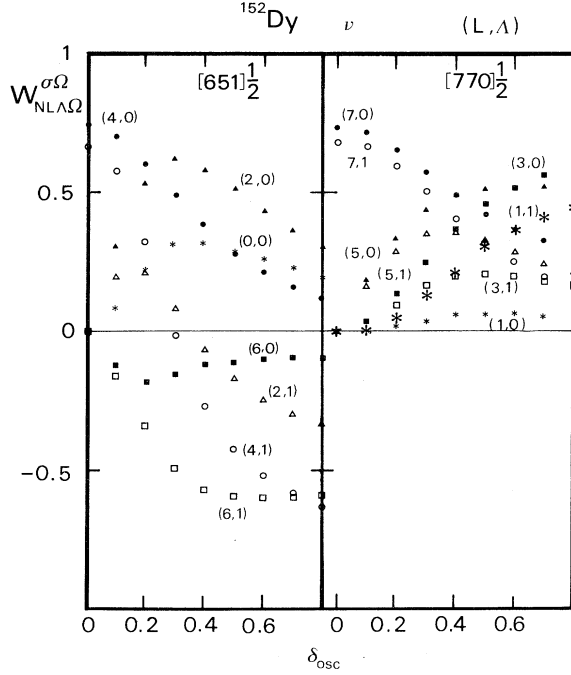


FIG. 9. The same quantities as in Fig. 8 for the neutron shell of ^{152}Dy . The filled (open) symbols denote the coefficients of $\Lambda = 0$ (1). For $[651]_{1/2}$, the circles correspond to $L=4$, the squares to $L=6$, the triangles to $L=2$ and the asterisks denote the contribution from $s1/2$ ($L=0, \Lambda=0$). For $[770]_{1/2}$, the circles correspond to $L=7$, the squares to $L=3$, the triangles to $L=5$, and the small asterisks denote the contribution from $p1/2$ ($L=1, \Lambda=0$), and the large asterisks denote the contribution from $p3/2$ ($L=1, \Lambda=1$).

this is usually much smaller than the other two elements provided that l is large. Thus, the couplings among the $j = l + \frac{1}{2}$ family members ($s1/2, d5/2, g9/2, \dots$, or $p3/2, f7/2, h11/2, \dots$) or among the $j = l - \frac{1}{2}$ family members ($d3/2, g7/2, \dots$, or $p1/2, f5/2, h9/2, \dots$) are strong, which keeps a j - j coupling scheme good. However the third matrix elements, i.e., those between spin-orbit partners of the spherical basis become almost comparable to the other two elements of Y_{20} for small values of l , such as $l=0$ and 1 ; that is, the coupling, for example, between $s1/2$ and $d3/2$ for positive parity levels or $p1/2$ and $p3/2$ for the negative parity levels. This fact causes strong mixing between the two families mentioned above, including large l value states after the diagonalization of the

whole matrix. In the last paper [7] we already showed the coefficients of the eigenvector in terms of the j - j spherical wave function, i.e., $W_{N,j,l,\Omega}^{\sigma,\Omega}$. In order to explain the reason more clearly, we show the matrix elements to be diagonalized for the case of $N=5$ and $\delta_{osc}=0.6$. The rows and columns correspond to the spherical single-particle levels from $p1/2, p3/2, f5/2, f7/2, h9/2$, and $h11/2$ in order,

$$\begin{pmatrix} 0 & -6 & -7 & 0 & 0 & 0 \\ -6 & -5 & -1 & -7 & 0 & 0 \\ -7 & -1 & -5 & -1 & -6 & 0 \\ 0 & -7 & -1 & -8 & 0 & -6 \\ 0 & 0 & -6 & 0 & -8 & 0 \\ 0 & 0 & 0 & -6 & 0 & -13 \end{pmatrix}. \quad (5)$$

These matrix elements include both of $1s$ and 1^2 interactions and all the values are measured from the first diagonal matrix element between $p1/2$ and $p1/2$. We see the strong coupling between $p1/2$ and $p3/2$, i.e., $\langle p1/2 | Y_{20} | p3/2 \rangle = -6$, while all the other matrix elements between the spin-orbit partners are very small, i.e., -1 or 0 . The eigenfunction of (5) has almost 50-50 mixed components between $j = l + \frac{1}{2}$ and $j = l - \frac{1}{2}$. Here we want to remark that in contrast to the case of pseudo-spin scheme where the $1s$ interaction is nearly zero, the $1s$ interaction remains large in the P - D levels, but the L - S coupling scheme becomes better than the j - j coupling scheme in the superdeformed limit, because of the large quadrupole deformed field. It is often pointed out that the deformed Woods-Saxon potential should be used rather than the deformed harmonic-oscillator potential. We anticipate that a similar situation occurs when the deformed Woods-Saxon potential is used. Namely a similar degeneracy of the P - D levels can be seen [10] and the L - S coupling scheme is recovered by the same argument concerning the mixture of $j = l + \frac{1}{2}$ and $j = l - \frac{1}{2}$ when superdeformed, which is shown in this section.

IV. THE EFFECT OF THE UNIQUE-PARITY LEVEL ON THE $M1$ TRANSMISSION

The difference between the pseudo-spin scheme ($\tilde{L}\tilde{S}$ coupling) and the real-spin one (L - S coupling) comes from the unique-parity level, as the pseudo-spin cannot include the unique-parity level. In order to see the difference between the two coupling schemes, we calculate the effect of the unique-parity level on the $M1$ transition rate. As it is linear in the spin operator, the $M1$ opera-

TABLE II. The squares of the $\Lambda = 0$ amplitudes and $\Lambda = 1$ amplitudes of the P - D levels in ^{152}Dy as a function of deformation.

| δ_{osc} | Proton | | | | Neutron | | | |
|----------------|--------------------------------|---------------|--------------------------------|---------------|--------------------------------|---------------|--------------------------------|---------------|
| | $[541]_{1/2}$ $\Lambda = 1$ | $\Lambda = 0$ | $[660]_{1/2}$ $\Lambda = 1$ | $\Lambda = 0$ | $[651]_{1/2}$ $\Lambda = 1$ | $\Lambda = 0$ | $[770]_{1/2}$ $\Lambda = 1$ | $\Lambda = 0$ |
| 0 | 0.43 | 0.57 | 0.46 | 0.54 | 0.44 | 0.56 | 0.47 | 0.53 |
| 0.2 | 0.23 | 0.77 | 0.42 | 0.58 | 0.27 | 0.73 | 0.44 | 0.56 |
| 0.4 | 0.54 | 0.46 | 0.28 | 0.72 | 0.40 | 0.60 | 0.34 | 0.66 |
| 0.6 | 0.78 | 0.22 | 0.15 | 0.85 | 0.69 | 0.31 | 0.19 | 0.81 |
| 0.8 | 0.89 | 0.11 | 0.08 | 0.92 | 0.84 | 0.16 | 0.09 | 0.91 |

tor is also a good physical quantity to test the recovery of the L - S coupling scheme. We calculated the matrix element of the following $M1$ transition operator.

$$\mu_x = g_l l_x + g_s s_x, \quad (6)$$

where the free nucleon values of g_l and g_s are assumed, i.e., $g_l = 1$ (0) and $g_s = 5.58$ (-3.82) for proton (neutron), respectively. The selection rule on transitions caused by the operator μ_x of (6) is $\Delta\sigma = 0$, $\Delta\alpha = 0$ and $\Delta\Omega = 0$ or ± 1 for the wave function $|\sigma, \Omega, \alpha\rangle$. The state $|\sigma, \Omega, \alpha\rangle$ is obtained by diagonalizing the Hamiltonian H in (1), but it is labeled for the sake of the convenience by the asymptotic wave function $[N, n_z, \Lambda\Omega]$ to which the state converges when δ_{osc} is extremely large. We show the calculated matrix elements of $\langle\sigma, \Omega, \alpha|\mu_x|\sigma', \Omega', \alpha\rangle$ and the contributions only from the unique-parity level for the wave function $|\sigma, \Omega, \alpha\rangle$ in Table III (proton shell) and Table IV (neutron shell) for the case of ^{152}Dy , and in Table V for the case of the neutron shell of ^{192}Hg . We choose only some typical examples in the tables in order to study the dependence of the contributions from the unique-parity level on the deformation. In the tables the numbers inside the parentheses denote the values only from the unique-parity level, including the direct [for example $(h11/2|\mu_x|h11/2)$] and crossing terms [$(h11/2|\mu_x|h9/2)$]. The numbers before the parentheses correspond to the total values of matrix elements of (6), in which all mixed states including the unique-parity states are taken into account. For example, for the diagonal matrix element of $[541]_{\frac{1}{2}}$, which is $[\tilde{4}\tilde{4}\tilde{0}]_{\frac{1}{2}}$ when the pseudo-spin representation is used, the contri-

bution of $h11/2$ is 0 at $\delta_{osc} = 0$, but reaches -0.56 at $\delta_{osc} = 0.6$, and its ratio to the total becomes 200%. The nondiagonal matrix element between $[541]_{\frac{1}{2}}$ and $[532]_{\frac{3}{2}}$ ($[\tilde{4}\tilde{4}\tilde{0}]_{\frac{1}{2}}$ and $[\tilde{4}\tilde{3}\tilde{1}]_{\frac{3}{2}}$ in pseudo-spin) has a 23% contribution of $h11/2$ at $\delta_{osc} = 0.2$, while at $\delta_{osc} = 0.6$ it becomes 70%. We drop the contribution from the unique-parity level, renormalize the wave function of $|\sigma, \Omega, \alpha\rangle$, and then estimate the $M1$ matrix elements produced by the pseudo-spin wave functions. We apply this method to both $[541]_{\frac{3}{2}}$ and $[530]_{\frac{1}{2}}$ in the superdeformed limit, as an example. Then the value of the diagonal matrix element $\langle i|M1|i\rangle$ for $[541]_{\frac{1}{2}}$ becomes 0.38, which should be compared with -0.28 in Table III. The nondiagonal matrix element $\langle i|M1|j\rangle$ between $[541]_{\frac{1}{2}}$ and $[530]_{\frac{1}{2}}$ is -1.44 in contrast to -2.23 in Table III. Thus, we cannot renormalize the wave function only within the pseudo-spin states ignoring the unique-parity level when the nucleus is superdeformed. On the other hand, the diagonal matrix element of the $[660]_{\frac{1}{2}}$ (unique-parity level at $\delta_{osc} = 0$) has 100% contribution from $i13/2$ at $\delta_{osc} = 0.0$, but reduces to 28.8% at $\delta_{osc} = 0.6$, which indicates that the pseudo-spin levels influence this state.

Similarly, in Table V, we see for the diagonal matrix element between $[770]_{\frac{1}{2}}$ that the contribution of $j15/2$ reduces from 100% to 16.8% at $\delta_{osc} = 0.6$, and in the nondiagonal transition matrix element between $[651]_{\frac{3}{2}}$ and $[613]_{\frac{5}{2}}$ ($[\tilde{5}\tilde{5}\tilde{2}]_{\frac{3}{2}}$ and $[\tilde{5}\tilde{1}\tilde{2}]_{\frac{5}{2}}$ in the pseudo-spin representation), the contribution of $i13/2$ to the total becomes very large at the superdeformed limit, i.e., -0.12 , while the total is -0.01 and its ratio is 12.0. As g_l is 0 for the neutron, the spin part of (6) only determines the $M1$ matrix

TABLE III. The contribution from the unique-parity level to the total single-particle $M1$ transition rate, $\langle\sigma, \Omega, \alpha|\mu_x|\sigma', \Omega', \alpha\rangle$ as a function of deformation for the proton shell in ^{152}Dy . The state $|\sigma, \Omega, \alpha\rangle$ is obtained by diagonalizing the total H , but is labelled by the asymptotic quantum numbers, $[N n_z \Lambda]\Omega$, to which the state converges in a very large deformation. The numerals inside of the parentheses denote the contribution from the unique-parity level to the total values, which are shown before the parentheses.

| δ_{osc} | 0.0 | 0.2 | 0.4 | 0.6 |
|---|------------|--------------|--------------|--------------|
| $\langle i M1 f\rangle$ | | | | |
| $[541]_{\frac{1}{2}} \rightarrow [541]_{\frac{1}{2}}$ | -3.31(0) | -2.88(-0.39) | -0.94(-0.51) | -0.28(-0.56) |
| $[541]_{\frac{1}{2}} \rightarrow [530]_{\frac{1}{2}}$ | 0(0) | -1.59(-0.52) | -2.42(-0.98) | -2.23(-1.17) |
| $[541]_{\frac{1}{2}} \rightarrow [510]_{\frac{1}{2}}$ | 1.13(0.0) | 0.45(0.23) | 0.13(0.42) | 0.05(0.53) |
| $[541]_{\frac{1}{2}} \rightarrow [532]_{\frac{3}{2}}$ | 3.20(0) | 2.13(0.49) | 1.23(0.76) | 1.26(0.88) |
| $[530]_{\frac{1}{2}} \rightarrow [541]_{\frac{3}{2}}$ | 1.35(1.35) | 0.99(0.37) | 0.08(-0.86) | -0.45(-1.20) |
| $[541]_{\frac{1}{2}} \rightarrow [541]_{\frac{3}{2}}$ | 0(0) | -1.20(-1.81) | -2.32(-2.22) | -2.77(-2.14) |
| $[541]_{\frac{3}{2}} \rightarrow [532]_{\frac{5}{2}}$ | 4.00(4.00) | 3.80(3.56) | 3.44(2.93) | 3.11(2.45) |
| $[541]_{\frac{3}{2}} \rightarrow [523]_{\frac{5}{2}}$ | 0(0) | -0.25(0.51) | -0.22(0.45) | -0.14(0.46) |
| $[660]_{\frac{1}{2}} \rightarrow [660]_{\frac{1}{2}}$ | 4.73(4.73) | 4.54(3.65) | 4.20(1.99) | 3.89(1.15) |
| $[660]_{\frac{1}{2}} \rightarrow [651]_{\frac{1}{2}}$ | 0(0) | -0.28(-1.72) | -0.33(-1.44) | -0.70(-0.99) |
| $[660]_{\frac{1}{2}} \rightarrow [651]_{\frac{3}{2}}$ | 4.68(4.68) | 4.45(3.72) | 3.81(2.27) | 3.18(1.44) |
| $[660]_{\frac{1}{2}} \rightarrow [622]_{\frac{3}{2}}$ | 0(0) | 0.12(-0.12) | 0.04(-0.26) | 0.01(-0.28) |

TABLE IV. The same quantities as in Table III for the neutron shell in ^{152}Dy .

| $\langle i M1 f\rangle$ | δ_{osc} | 0.0 | 0.2 | 0.4 | 0.6 |
|---|----------------|--------------|--------------|--------------|--------------|
| $[651]_{\frac{1}{2}} \rightarrow [651]_{\frac{1}{2}}$ | | -1.06(0) | -1.46(-0.05) | -1.14(0.07) | -0.60(0.10) |
| $[651]_{\frac{1}{2}} \rightarrow [611]_{\frac{1}{2}}$ | | 0(0) | -0.14(-0.06) | -0.03(-0.10) | -0.01(-0.11) |
| $[651]_{\frac{1}{2}} \rightarrow [620]_{\frac{1}{2}}$ | | 0.95(0) | 0.52(0.16) | 0.16(0.23) | 0.05(0.24) |
| $[651]_{\frac{1}{2}} \rightarrow [631]_{\frac{3}{2}}$ | | 0(0) | -0.43(-0.29) | -0.52(-0.53) | -0.27(-0.64) |
| $[651]_{\frac{1}{2}} \rightarrow [642]_{\frac{3}{2}}$ | | -1.04(0) | -0.71(-0.11) | 0.32(-0.17) | 0.54(-0.17) |
| $[640]_{\frac{1}{2}} \rightarrow [651]_{\frac{3}{2}}$ | | -1.10(-1.10) | -1.09(-0.71) | -0.87(-0.15) | -0.63(-0.05) |
| $[651]_{\frac{3}{2}} \rightarrow [642]_{\frac{5}{2}}$ | | -0.98(-0.98) | -0.95(-0.86) | -0.83(-0.66) | -0.68(-0.49) |
| $[651]_{\frac{3}{2}} \rightarrow [613]_{\frac{5}{2}}$ | | 0(0) | -0.04(-0.13) | -0.02(-0.13) | -0.01(-0.12) |
| $[770]_{\frac{1}{2}} \rightarrow [770]_{\frac{1}{2}}$ | | 1.02(1.02) | 1.06(0.81) | 1.27(0.46) | 1.55(0.26) |
| $[770]_{\frac{1}{2}} \rightarrow [761]_{\frac{1}{2}}$ | | 0(0) | 0.12(-0.35) | 0.56(-0.25) | 0.66(-0.14) |
| $[770]_{\frac{1}{2}} \rightarrow [761]_{\frac{3}{2}}$ | | -1.01(-1.01) | -1.03(-0.82) | -0.96(-0.48) | -0.76(-0.27) |
| $[770]_{\frac{1}{2}} \rightarrow [752]_{\frac{3}{2}}$ | | 0(0) | 0.16(-0.29) | 0.38(-0.17) | 0.31(-0.02) |

element, and the dependence of the unique-parity on the deformation can be clearly seen. On the other hand, in the proton case the orbital part of (6) also affects the dependence and sometimes cancels the spin part so as to smear out the effect. This is the reason why the contribution from the unique-parity is more clearly seen in the neutron case than the proton case for superdeformed nuclei.

Recently dipole transitions linking signature partner superdeformed bands in ^{193}Hg are observed [11]. The assigned levels in Ref. [11] are $[512]_{\frac{5}{2}}$ and $[624]_{\frac{9}{2}}$, both of which do not belong to the $N_{sh} = 8$, but the former to $N_{sh} = 9$ and the latter to 10 at superdeformation. In Table V we showed some calculated matrix elements for both $[512]_{\frac{5}{2}}$ and $[624]_{\frac{9}{2}}$ levels together with those for the members of $N_{sh} = 8$, i.e., $[532]_{\frac{5}{2}}$, $[642]_{\frac{5}{2}}$, $[761]_{\frac{1}{2}}$, $[761]_{\frac{3}{2}}$,

TABLE V. The same quantities as in Table III for the neutron shell in ^{192}Hg .

| $\langle i M1 f\rangle$ | δ_{osc} | 0.0 | 0.2 | 0.4 | 0.6 |
|--|----------------|--------------|--------------|--------------|--------------|
| $[631]_{\frac{3}{2}} \rightarrow [642]_{\frac{5}{2}}$ | | -1.25(-1.25) | -0.86(-0.55) | -0.56(-0.14) | -0.40(0.01) |
| $[642]_{\frac{5}{2}} \rightarrow [613]_{\frac{7}{2}}$ | | 0.51(0.51) | 0.11(0.31) | 0.04(0.29) | 0.02(0.26) |
| $[613]_{\frac{7}{2}} \rightarrow [624]_{\frac{9}{2}}$ | | -1.54(-1.54) | -0.53(-0.45) | -0.33(-0.23) | -0.24(-0.14) |
| $[624]_{\frac{9}{2}} \rightarrow [606]_{\frac{11}{2}}$ | | 0.21(0.21) | 0.13(0.17) | 0.08(0.15) | 0.06(0.15) |
| $[880]_{\frac{1}{2}} \rightarrow [880]_{\frac{1}{2}}$ | | -1.01(-1.01) | -1.03(-0.86) | -1.14(-0.54) | -1.40(-0.28) |
| $[880]_{\frac{1}{2}} \rightarrow [862]_{\frac{3}{2}}$ | | 0(0) | -0.11(0.28) | -0.36(0.23) | -0.39(0.07) |
| $[541]_{\frac{3}{2}} \rightarrow [512]_{\frac{5}{2}}$ | | 0.60(0.60) | 0.14(0.39) | 0.04(0.35) | 0.02(0.30) |
| $[541]_{\frac{3}{2}} \rightarrow [523]_{\frac{5}{2}}$ | | 0(0) | -0.40(-0.34) | -0.24(-0.27) | -0.14(-0.24) |
| $[512]_{\frac{5}{2}} \rightarrow [523]_{\frac{7}{2}}$ | | -1.47(-1.47) | -0.55(-0.44) | -0.35(-0.22) | -0.25(-0.12) |
| $[523]_{\frac{5}{2}} \rightarrow [523]_{\frac{7}{2}}$ | | 0(0) | 1.54(1.46) | 1.71(1.53) | 1.79(1.55) |
| $[761]_{\frac{1}{2}} \rightarrow [732]_{\frac{3}{2}}$ | | 0(0) | -0.37(-0.05) | -0.23(-0.05) | -0.09(0.00) |
| $[761]_{\frac{3}{2}} \rightarrow [743]_{\frac{5}{2}}$ | | 0(0) | -0.16(0.18) | -0.33(0.04) | -0.28(-0.07) |

and $[880]_{\frac{1}{2}}$. We see the effect of the unique-parity contribution becomes important according with increasing deformation even for $[523]_{\frac{5}{2}}$ and $[642]_{\frac{5}{2}}$ levels which are not the members of $N_{sh} = 8$. These matrix elements in Table V do not correspond to the transitions linking the signature partners except for the diagonal matrix element in $[880]_{\frac{1}{2}}$. We will publish the realistic calculation on the linking transitions between the signature partners of ^{193}Hg in the future.

It is seen from the tables that the effect of the unique-parity level becomes very important when superdeformed. The states, for which the pseudo-spin states dominate at small deformation, are much affected by the contribution from the unique-parity level, while the states for which the unique parity states dominate at small deformation get a non-negligible contribution from the pseudo-spin states. This means the $M1$ transition probabilities, which are proportional to the squares of transition matrix elements, are very much affected by the mixing of unique parity states and pseudo-spin states.

Another difference between the present real-spin mechanism and the pseudo-spin mechanism in the explanation of the quantization of alignment at superdeformation is that the real-spin mechanism has both the same parity and the different parity states degenerate, because of the relation $N_{sh} = 2N - n_z$, while the pseudo-spin mechanism has only states with the same parity degenerate. Thus, if two particles are occupying two almost degenerate different parity levels, total alignment can take 0 or 1 and total parity can be either + or -. The $M1$ transition is allowed between the excited superdeformed bands with the same parity levels, while an $E1$ transition is allowed between the two excited superdeformed bands with the different parity. If one particle is inserted in these degenerate levels, again + and - parity excited bands are possible with an alignment of $\frac{1}{2}$. The twin bands and also the incremental alignment [1] may come from this mechanism. Once the transition between the excited superdeformed bands is observed, we can distinguish which is the case. In the case of pseudo-spin, only the same parity excited bands are allowed, and only an $M1$ transition between them is allowed. Even when this is the case, we emphasize that the $M1$ matrix elements are greatly modified by the mixture of unique-parity levels.

V. CONCLUSION

We show the following conclusions from the numerical analyses based on the realistic calculation in Secs. II, III, and IV. Not only the P - D levels, but also some levels belonging to the same N_{sh} are well approximated around the superdeformed limit by the asymptotic wave functions. Although the expectation values of the spin-orbit

interaction by the unique-parity partner of the P - D levels do not converge sufficiently to the asymptotic values, their L - S coupled spherical wave function components become more than 85% of the total. We find that this is due to the nature of the large quadrupole deformed field δY_{20} . Since the $N_{sh} = 6(7)$ for the proton shell and $7(8)$ for the neutron shell, including the P - D levels, are located near the fermi surface of ^{152}Dy (^{192}Hg), i.e., reference systems in the discussion of the quantization of alignment, we can use real spin “ s ” instead of the pseudo-spin “ \tilde{s} ” at superdeformation because of the restored L - S coupling scheme. Among all the levels belonging to the N_{sh} , the P - D levels are the best candidates to explain the quantization of alignment. As both positive and negative parity levels are degenerate in the P - D levels, two particles excited from the reference system into such P - D levels will produce one or zero aligned bands with both parities. This mechanism should explain the existence of twin bands.

It should be pointed out that the real-spin mechanism works only in the superdeformed limit, as it is related with the shell structure. On the other hand, the pseudo-spin works at any deformation. Therefore the quantization of alignment observed for normal deformation [2] cannot be explained by this real-spin mechanism and may be explained in the frame of pseudo-spin mechanism or some other theory. As for the quantization of alignment for $A \sim 130$ [3] at $\delta_{osc} \sim 0.375$, we obtain the same conclusion as for $A \sim 150$, if the rotational frequency for $A \sim 130$ is as small as for $A \sim 150$. However, the rotational frequency is very large in this region, $0.9 \geq \hbar\omega_{rot} \geq 0.5$. It is very difficult to see how the L - S coupling or pseudo \tilde{L} - \tilde{S} coupling can still work in such a high rotational frequency. This is still an open problem for future discussion. Next the pseudo-spin mechanism uses only the degeneracy of the same parity levels, while the real-spin mechanism uses the degeneracy of the different parity levels. Thus, the excited superdeformed bands can have both possibilities of + and - parities. The transition connecting these excited superdeformed bands can be either $E1$ or $M1$ and $E2$ transitions. On the other hand, if the pseudo-spin mechanism is responsible for the identical bands, both bands have the same parity and only $M1$ and $E2$ transitions can occur. Finally, it should be pointed out that the unique-parity level must be separately discussed in the pseudo-spin formalism, while the real-spin mechanism can take into account both the unique-parity states and the pseudo-spin states on the equal footing. We calculate the effect of unique-parity components on $M1$ transition rates and find that they become very important with increasing deformation.

The authors express their sincere thanks to Prof. B. R. Barrett for his careful reading of this manuscript.

-
- [1] F. S. Stephens *et al.*, Phys. Rev. Lett. **65**, 301 (1990).
 [2] C. Baktash, J. D. Garrett, D. F. Winchell, and A. Smith, Phys. Rev. Lett. **69**, 1500 (1992).
 [3] J. Gizon, talk at the XIth International School on Nu-

clear Physics and Neutron Energy, Varna, Bulgaria, 1993 (unpublished).

- [4] C. Gustafson, I. L. Lamm, B. Nilsson, and S. G. Nilsson, Ark. Fys. **36**, 613 (1967).

- [5] A. Arima, M. Harvey, and K. Shimizu, *Phys. Lett.* **30B**, 517 (1969).
- [6] K. T. Hecht and A. Adler, *Nucl. Phys.* **A137**, 129 (1969).
- [7] K. Sugawara-Tanabe and A. Arima, *Phys. Lett. B* **317**, 1 (1993); *Nucl. Phys.* **A557**, 157C (1993).
- [8] T. Bengtsson, I. Ragnarsson, and S. Åberg, *Computational Nuclear Physics* **1**, 51 (Springer-Verlag, Berlin, 1991).
- [9] S. G. Nilsson, *K. Dan Vidensk. Selsk. Mat.-Fys. Medd.* **29**, No. 16 (1955).
- [10] A. Gelberg, private communication.
- [11] M. J. Joyce *et al.*, *Phys. Rev. Lett.* **71**, 2176 (1993).